

Multi-harmonic EMI reduction optimization of spread spectrum in multiple-RBW environment

*Original*

Multi-harmonic EMI reduction optimization of spread spectrum in multiple-RBW environment / Gabriele, Francesco; Pareschi, Fabio; Lena, Davide; Rosa Borghi, Maria; Rovatti, Riccardo; Setti, Gianluca. - In: IEEE TRANSACTIONS ON CIRCUITS AND SYSTEMS. I, REGULAR PAPERS. - ISSN 1558-0806. - STAMPA. - 72:7(2025), pp. 3488-3497. [10.1109/TCSI.2025.3549360]

*Availability:*

This version is available at: 11583/2998415 since: 2025-08-07T10:16:27Z

*Publisher:*

IEEE

*Published*

DOI:10.1109/TCSI.2025.3549360

*Terms of use:*

This article is made available under terms and conditions as specified in the corresponding bibliographic description in the repository

*Publisher copyright*

IEEE postprint/Author's Accepted Manuscript

©2025 IEEE. Personal use of this material is permitted. Permission from IEEE must be obtained for all other uses, in any current or future media, including reprinting/republishing this material for advertising or promotional purposes, creating new collecting works, for resale or lists, or reuse of any copyrighted component of this work in other works.

(Article begins on next page)

# Multi-harmonic EMI reduction optimization of spread spectrum in multiple-RBW environment

Francesco Gabriele, *Graduate Student Member, IEEE*, Fabio Pareschi, *Senior Member, IEEE*, Davide Lena, Maria Rosa Borghi, Riccardo Rovatti, *Fellow, IEEE*, and Gianluca Setti, *Fellow, IEEE*

**Abstract**—We investigate here both from a theoretical and practical point of view the problem of optimizing EMI reduction by means of spread spectrum clocking when lower harmonics need to be analyzed with a smaller RBW, and higher harmonics with a larger one. This situation is indeed a trade-off, where a designer can trade performance in terms of EMI reduction for lower harmonics with that achieved for higher harmonics. Two approaches are considered and analyzed. **The first trade-off, denoted as Single Triangular Modulation, consists in the standard and commonly adopted triangular based spreading, where the role of the parameters is investigated with the aim of optimizing EMI reduction both in the lower part and the upper part of the spectrum. The second one, denoted as Double Triangular Modulation, is inspired by a recent Application Note and it is much more complex from an implementation point of view, being based on two simultaneous triangular modulations with different parameters. The comparison shows very similar performance, so that the adoption of the more complex approach results questionable.**

**Index Terms**—ElectroMagnetic Interferences, Spread spectrum, Frequency Modulation, DC-DC converters.

## I. INTRODUCTION

**S**PREAD SPECTRUM is a well known technique first introduced in [1], [2] to mitigate the problem of Electromagnetic Interference (EMI) emissions in all electronic circuits presenting any switching activity, such as digital circuits, switching DC-DC converters, communication protocols, and others. With EMI we refer to an *unintentional* energy transfer from a source circuit to a victim circuit either by means or electromagnetic radiation or as disturbances propagated through the power supply line, that may cause a malfunctioning in the victim. To avoid this scenario, international regulations [3], [4] state that the emitted power spectrum of any commercial device, measured in the proper way [5], should present a density peak below a given level. In accordance to this point of view, spread spectrum clocking technique introduces a controlled jitter in the interfering signal with the aim of introducing additional spectral components, thus reducing the energy of components already present in the spectrum.

Spread spectrum is quite common nowadays, and many references can be found in the literature [6]–[9], including

F. Gabriele and F. Pareschi are with the DET, Politecnico di Torino, 10129 Torino, Italy (e-mail: {francesco.gabriele, fabio.pareschi}@polito.it

D. Lena and M. R. Borghi are with STMicroelectronics s.r.l. – Torino, Italy. (email: {davide.lena, maria-rosa.borghi}@st.com).

R. Rovatti is with the DEI, University of Bologna, 40136 Bologna, Italy (e-mail: riccardo.rovatti@unibo.it).

G. Setti is with CEMSE, King Abdullah University of Science and Technology (KAUST), Saudi Arabia (e-mail: gianluca.setti@kaust.edu.sa).

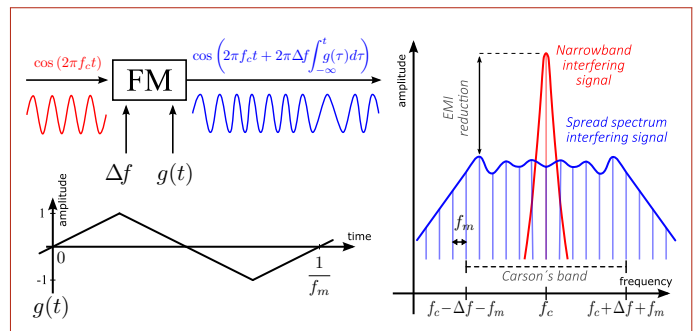


Fig. 1. Applying Spread Spectrum to a sinusoidal tone redistributes its energy so that energy spectrum is changed from narrow-band to wide-band, with a reduction in its peak level. Even when considering periodic signals with a theoretical discrete spectra (faded lines on the right panel), the measured EMI spectra will appear continuous (solid lines) due limitations in the EMI measurement set-up both for the unmodulated and the modulated case.

some overview works [10], [11]. Applications range from LED lighting [12], [13] to induction heating [14], communication protocol such as PCIexpress or Serial-ATA [15], GaN based-converters either for automotive [16] or low-power commercial converters [17], and even to modular converters for space applications [18]. Some works exist also investigating the relation between EMI and a DC-DC output ripple [19], or how to implement spreading in a full-digital PWM [20]. Spread spectrum can also be found in many commercial DC-DC switching converters [21], [22].

Even if many different approaches exist [10], the most common way to implement spreading is by means of a *Frequency Modulation* (FM) of the reference timing signal by means of a driving signal  $g(t)$ , as schematized in Figure 1. In fact, modulating the reference timing signal is the easiest way to modulate all synchronous signals with it (e.g., the input current signal is in-phase with the reference clock of the pulse-width modulator stage in a DC-DC converter).

The modulation of a sinusoidal tone at frequency  $f_c$  with a periodic driving signal  $g(t)$  at frequency  $f_m$  is sketched in Figure 1. We know that: *i*) the resulting spectrum is periodic, but appears as continuous due to limitation in the measurement setup; *ii*) according to Carson's rule [23], modulation results in a spread of the power of the signal approximately in a band  $[f_c - \Delta f - f_m, f_c + \Delta f + f_m]$ , where  $\Delta f$  is the frequency deviation; *iii*) depending on the signal profile of  $g(t)$ , different shapes of the modulated signal spectrum are obtained. For instance, the adoption of a sinusoidal driving signal implies the presence of two peaks at both ends of

Carson's bandwidth [10]. Therefore, despite it can be easily synthesized in hardware, its adoption results in non-optimum EMI-reduction performances. Many other approaches have drawn the attention of designers, including random, pseudo-random or even chaotic modulations [10], [24], [25]. However, even if these solutions ensure very good EMI reduction performance, they require complex hardware designs to generate the signal  $g(t)$ . In contrast, the adoption of a triangular driving signal represents a very good trade-off between the signal generation complexity and the flatness of the modulated signal spectrum. For such a reason, it results the most common modulation approach for EMI reduction purposes. Indeed, a triangular  $g(t)$  ensures that the spectrum in the Carson's band is almost flat, independently of  $f_m$ . Since it is intuitive that the flatter the power spectrum in a given band is, the lowest its peak value, it is clear how this solution ensures the highest probability to be complaint with regulations. In conjunction, a triangular signal can be straightforwardly generated through simple analog or digital circuital implementations [26], [27].

Due to aforementioned properties, the spread spectrum based on triangular modulation has been intensively studied from a theoretical point of view. Authors of [28] were able to analytically compute both the theoretical Fourier spectrum (i.e., the spectrum computed according to the Fourier Transform), and the expected spectrum when measured in accordance to the EMI regulations (that will be hereinafter referred as EMI spectrum). Even if the Fourier spectrum of a spread signal is almost flat in the Carson's band, in particular for small values of  $f_m$ , the EMI reduction measured with a spectrum analyzer (as in accordance to regulations) coincides with the EMI reduction expected according to the Fourier spectrum only for high  $f_m$  values, whereas we can see a reduction in the effectiveness of spreading with respect to what expected from the Fourier spectrum when the modulation frequency  $f_m$  is low. This is due to the so-called *short-time effect*, and the intuitive explanation is that when the interfering signal frequency is changed too slowly, it appears to any victim circuit (and also to the spectrum analyzer) indistinguishable from an unmodulated signal. In other words, spreading fails if observed for a short-time period (that happens when the victim circuit has a fast transient response to such an interference). Accordingly, optimal performance in terms of EMI reduction is for a finite value of  $f_m$ , that has been found in [28] to be similar to the resolution bandwidth (RBW) used in the spectrum analyzer and imposed by regulations.

For a generic interfering signal, the above observations on a sinusoidal tone can be done for any of its harmonics. Interestingly, when a unique RBW value is considered, optimum in terms of EMI reduction is achieved at the same time for all harmonics. Due to this, it is very common when dealing with spread spectrum clocking to limit the investigation to a sinusoidal interfering signal only.

However, if the EMI reduction optimization process involves multiple frequency windows featuring different RBWs, the results in [28] do not directly apply. In fact, international regulations such as [5] require that the RBW to be used is changed when scanning different parts of the power spectrum. As an example, the RBW is 9 kHz for frequency up

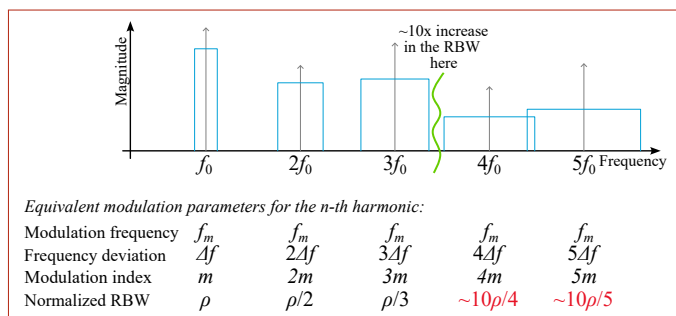


Fig. 2. Example of the scenario considered in this paper, where the RBW has to be changed (approx. increased of one order of magnitude) between lower and higher harmonics. Equivalent parameters regulating the modulation of the different harmonics (detailed in Section II) are also listed.

to 30 MHz, but has to be increased to 120 kHz for higher frequencies. If the analyzed bandwidth is further increased above 1 GHz, than the required RBW is 1 MHz. Generally, an increase of approximately of one order of magnitude is observed from one EMI band to another one.

The effect of this can be observed in the example of Figure 2, where the RBW has to be changed between the third and the fourth harmonics. The key point, mathematically detailed in Section II, is that one can handle the modulation of a complex signal such as a PWM one simply by modulating each of its harmonics with a different set of equivalent parameters, the most important of which are also reported in the figure. As can be observed, the change in the RBW generates a discontinuity in the normalized RBW, defined as the RBW divided by the equivalent frequency deviation. This makes the optimization procedure for the lower harmonics completely different from that for higher harmonics, and also paves the way to a joint optimization procedure never considered in the spread-spectrum related literature.

This situation is of practical industrial interest, and it has been considered in a recent Application Note [29]. The latter investigates EMI compatibility of high-speed DC-DC converters operating with a switching frequency in the several MHz range, where only a few harmonics of the switching frequency require a 9 kHz RBW, the 120 kHz RBW has to be used for higher harmonics. It is clear that EMI optimization in this scenario is much more complex than simply setting  $f_m = \text{RBW}$ , as this approach only optimizes either the lower harmonics in the spectrum or the higher harmonics.

To cope with this case, a particular spreading approach has been proposed in [29] based on two simultaneous modulations, one using a low frequency driving signal and the other using a high frequency driving signal. It has been empirically shown through bench measurements that this technique is effective in mitigating the disturbances in both frequency ranges. However, it completely lacks both a theoretical foundation and a comparison with other suitable approaches for the EMI reduction purposes in a multiple RBWs environment.

Hence, the scope of this work is twofold. First, we want to establish a theoretical framework for the approach presented in [29]. As it will be thoroughly detailed, this practically translates in addressing the problem of the spectrum computation

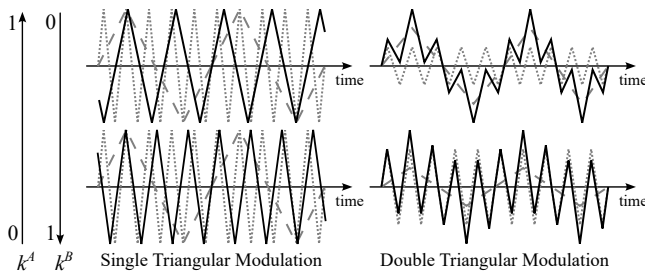


Fig. 3. The two spread spectrum approaches considered in this paper: the **Single Triangular Modulation** (left) and the **Double Triangular Modulation** (right). The former relies on a triangular waveform (solid plots) at a frequency intermediate between a lower one (dashed plots) and a higher one (dotted plots) according to two coefficients  $k^A \in [0, 1]$  and  $k^B = 1 - k^A$ . The latter involves the weighted sum (solid plots) of a low frequency triangular waveform (dashed plots) and a high frequency triangular waveform (dotted plots) according to the same two coefficients.

of the cascade of two generic frequency modulations, making the computation of the resulting spectrum much easier than a direct computation. Due to the practical reasons discussed above, we focus on both FMs generated by triangular driving signals, instead of employing one triangular and one random modulation as in [29]. This method, sketched in Figure 3, will hereinafter be referred as **Double Triangular Modulation (DTM)**.

Second, we will compare the DTM approach with a simpler one, which we name **Single Triangular Modulation (STM)**, and also shown in Figure 3. The latter involves a single triangular waveform with an optimized modulation frequency value  $f_m$ , which turns out to be an intermediate value between the two RBWs values to be used. In both the examined cases, the optimization process will result in a trade-off between the EMI reduction for lower harmonics (i.e., harmonics in the low-RBW frequency region) and for higher ones (i.e., harmonics in the high-RBW frequency region). It will be demonstrated that the DTM approach has only limited advantages with respect to the optimized STM. Consequently, *this makes questionable* the adoption of two simultaneous modulations in practical cases.

The paper is organized as follows. In Section II, an essential mathematical background for multi-harmonic spread spectrum is provided. In Section III, the STM approach in a multi-RBWs scenario is considered, detailing the derivation of the theoretical and measured spectra, and experimentally validating the achieved results. In Section IV, the case of spreading by means of DTM waveforms is considered. In Section V, some comments regarding the comparison between the STM and the DTM approaches are proposed, describing the trade-offs introduced with these two approaches. Finally, we draw the conclusion.

## II. SPREAD SPECTRUM MATHEMATICAL BACKGROUND

Let us consider a generic periodic signal  $s(t)$  representing the main source of EMI, such as, for example, the conducted power supply current in a DC-DC converter. Being the system periodic of frequency  $f_c$ , let us assume to write  $s(t)$  as

$$s(t) = A\Psi(2\pi f_c t) = A\Psi(\phi(t)) \quad (1)$$

where  $A$  is the signal amplitude,  $\Psi$  is a proper function normalized in amplitude (i.e., so that  $-1 < \Psi(\phi) < 1$ ) and periodic with unitary angular frequency (i.e., with a  $2\pi$  period), whereas  $\phi(t) = 2\pi f_c t$  is the instantaneous phase of the signal, and  $d\phi/dt = 2\pi f_c$  the instantaneous angular frequency.

Let us also consider a normalized periodic signal  $-1 \leq g(\xi) \leq 1$  with unitary angular frequency and zero average, i.e.,  $\int_0^{2\pi} g(\xi) d\xi = 0$ . We want to apply FM to  $\Psi$  using frequency deviation  $\Delta f$  and driving signal  $g(2\pi f_m t + \varphi)$ . Applying a FM is basically a change in the instantaneous phase from  $\phi$  to  $\phi'$  according to the modulation law:

$$\phi'(t) = \phi(t) + 2\pi\Delta f \int_{-\infty}^t g(2\pi f_m \tau + \varphi) d\tau, \quad (2)$$

where the new instantaneous angular frequency is  $d\phi'/dt = 2\pi f_c + 2\pi\Delta f g(2\pi f_m t + \varphi)$ , ranging from  $2\pi(f_c - \Delta f)$  to  $2\pi(f_c + \Delta f)$ . Note that this observation is grounding the aforementioned Carson's rule, and it is also in accordance with the example of Figure 1. Since FM is achieved by altering the phase of a signal, it is reasonable to assume that when applying the spreading to the reference timing signal, all the signals generated starting from this one share the same phase, and so they are modulated according to the same law. This is the approach commonly followed in actual spread spectrum clocking implementations.

From (2), we can infer some information regarding the obtained spectrum. In particular, assuming  $\Psi$  has a Fourier expansion

$$\Psi(\phi) = \psi_0 + \psi_1 \cos(\phi + \varphi_1) + \psi_2 \cos(2\phi + \varphi_2) + \dots, \quad (3)$$

and applying the series expansion (3) and the modulation law (2) to (1), the generic  $n$ -th harmonic of  $s(t)$  reads as

$$A\psi_n \cos\left(2\pi n f_c t + 2\pi n \Delta f \int_{-\infty}^t g(2\pi f_m \tau + \varphi) d\tau + \varphi_n\right). \quad (4)$$

This leads to the common knowledge that applying FM to a generic signal is equivalent to independently modulate each of its harmonic, the  $n$ -th harmonic modulated with a frequency deviation  $n\Delta f$  and the same driving signal  $g(2\pi f_m t + \varphi)$ .

Thanks to this, in order to study the FM of a generic signal, it is enough to consider the FM of a generic sinusoidal tone and apply the results to all harmonics of the generic signal. As an example, Figure 2 shows how parameters change for the first five harmonics of a generic signal. For the sake of simplicity, we will limit ourselves to consider the modulation of a sinusoidal tone, i.e.,  $\Psi(\phi(t)) = \cos(\phi(t))$ , without considering phase and amplitude parameters (i.e., according to the established notation in (4),  $A = 1$  and  $\varphi_1 = 0$ ) and applying different modulation parameters depending on the harmonic we will consider, as shown in Figure 2.

## III. SINGLE TRIANGULAR MODULATION

In the following, we will quickly recall some of the properties and formulas grounding the analytic computation of the spectrum of a frequency modulated signal, which will allow

us to better understand some properties of spread spectrum systems.

**Fourier Spectrum:** let us define the auxiliary function

$$G(\tau) = \int_{-\infty}^{\tau} g(\xi) d\xi, \quad (5)$$

that, given the properties of  $g$ , is periodic with a unitary angular frequency period. Being  $j$  the imaginary unit and introducing the parameter  $m \in \mathbb{R}$ , also the function  $e^{jmG(\tau)}$  exhibits periodicity with a unitary angular frequency. Therefore, it can be written as the Fourier complex series

$$e^{jmG(\tau)} = \sum_{l=-\infty}^{+\infty} \Gamma_l(m) e^{jl\tau}, \quad (6)$$

where  $\Gamma_l(m)$  is a proper sequence of complex numbers depending on  $m$ , computed as

$$\Gamma_l(m) = \frac{1}{2\pi} \int_{-\pi}^{\pi} e^{jmG(\tau)} e^{-jl\tau} d\tau. \quad (7)$$

It is easy to see that, if  $G$  is an odd function (i.e.,  $G(-\xi) = -G(\xi)$ ), then  $\Gamma_l(m) \in \mathbb{R}$ .

The computation of the Fourier spectrum for a modulated sinusoidal tone assuming a generic driving signal  $g$  can be derived from the sequence  $\Gamma_l(m)$  in the same ways used in textbooks [23] when the driving signal is a sinusoidal tone, namely:

$$\begin{aligned} \Psi(\phi(t)) &= \cos\left(2\pi f_c t + 2\pi \Delta f \int_{-\infty}^t g(2\pi f_m \tau + \varphi) d\tau\right) = \\ &= \text{Re}\left(e^{j2\pi f_c t} e^{jmG(2\pi f_m t + \varphi)}\right) = \\ &= \text{Re}\left(e^{j2\pi f_c t} \sum_{l=-\infty}^{+\infty} \Gamma_l(m) e^{jl\varphi} e^{j2\pi l f_m t}\right) = \\ &= \sum_{l=-\infty}^{+\infty} |\Gamma_l(m)| \cos(2\pi f_c t + 2\pi l f_m t + \arg(\Gamma_l(m)) + l\varphi), \end{aligned} \quad (8)$$

where  $\text{Re}$  is the real part operator and  $m = \Delta f / f_m$  is a secondary parameter usually addressed to as *modulation index*.

As well known in modulation theory, the power spectrum of (8) is discrete, with components at frequencies  $f_c + l f_m$ ,  $l \in \mathbb{Z}$ , whose amplitude depends on  $|\Gamma_l|$  only, and phase on  $\arg(\Gamma_l)$  and  $\varphi$ . As already observed, for a non-sinusoidal  $s(t)$ , it is enough to apply (8) to each of its harmonics, considering a different modulation index as in Figure 2 and, according to (4), an amplitude scaling by  $A\psi_n$  and a phase lag  $\varphi_n$ .

The computation of the  $\Gamma_l(m)$  in (7) is fairly intricate. The case of a sinusoidal modulation (i.e.,  $g(\xi) = \cos(\xi)$  and so  $G(\xi) = \sin(\xi)$ ) is well known [23], with  $\Gamma_l(m) = J_l(m)$  real and given by the Bessel functions of first kind and order  $l$ . The case of a triangular modulation has been solved in [28], and assuming

$$g(\xi) = \begin{cases} 1 + 2\frac{\xi - 2k\pi}{\pi}, & \text{if } -\pi + 2k\pi < \xi < 2k\pi \\ 1 - 2\frac{\xi - 2k\pi}{\pi}, & \text{if } 2k\pi < \xi < \pi + 2k\pi \end{cases} \quad (9)$$

with  $k \in \mathbb{Z}$ , leads again to real coefficients  $\Gamma_l(m)$ . The case of a driving signal made of pulses with random amplitudes

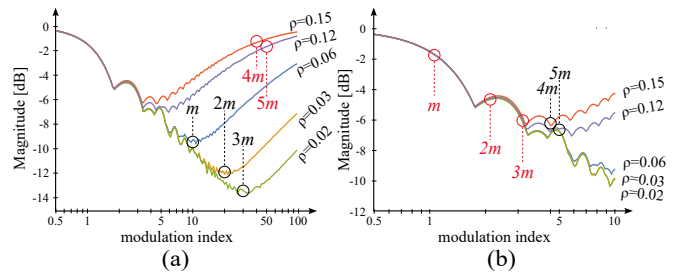


Fig. 4. Different optimization possibilities for a standard spreading approach for the case study of Figure 2. (a): Optimization of lower-order harmonics; and (b): Optimization of higher-order harmonics.

has been analytically studied in [30]. This case is however slightly different since it leads, due the lack of periodicity, to a continuous spectrum. To the best of authors' knowledge, no other cases of interest have been analytically solved. **In this regard, under the assumption of an arbitrary-shaped  $g(\xi)$ , deriving an analytical closed-form expression for the  $\Gamma_l(m)$  coefficients directly via (7) is not straightforward.**

**EMI spectrum:** it was observed in [28] that the EMI spectrum (i.e., the spectrum measured by the spectrum analyzer) of a sinusoidal tone modulated by means of a triangular driving signal is different from what expected according to the aforementioned Fourier spectrum. First of all, the former is a continuous spectrum measured with a limited resolution, whereas the latter is discrete and achievable by measurements only if assuming an infinitely high resolution. It is evident that a straightforward comparison is not possible. A comparison is indeed possible if one consider the spectrum achieved when assuming that the discrete Fourier spectrum is observed with a resolution that is limited, and equal to the RBW. This is point of view considered in [28] and, accordingly, the Fourier-derived spectrum decreases with  $m$  until the product between the modulation index and the the normalized instrument resolution, defined as  $\rho = \text{RBW} / \Delta f$ , is such that  $m\rho \gg 1$ . In this case, the resolution of the instrument  $\text{RBW} \gg f_m$ , i.e., it is not enough to detect the individual spectral components, and the power of many of them is summed in the observed spectrum. Assuming a flat spectrum in the Carson's band, the achieved EMI reduction (defined, as in the example of Figure 1, as the difference between the peak value of the power spectrum of an unmodulated signal and the peak value of the measured power spectrum of the same signal when spreading is applied) is given by  $10 \log(\text{RBW} / (2\Delta f)) = 10 \log(\rho/2)$ .

If we compare this spectrum with the EMI one, we can say that when  $m$  is low (approximately,  $m\rho < 1$ ) the two spectra are very similar, whereas for high values of  $m$  (i.e., approximately  $m\rho > 1$ ) many differences arise. In particular, the EMI spectrum for  $m$  very large is increased to almost the same value of the unmodulated spectrum, leading to no reduction in terms of EMI. Motivations are deeply discussed in [28]. In other word, if EMI reduction for the Fourier-derived spectrum is achieved for large  $m$ , this does not happen for the EMI spectrum. When considering international regulations, according to [28], the EMI reduction is a function  $R^{\text{EMI}}(m, \rho)$  depending on  $m$  and  $\rho$  only. In order to maximize the actual



the fifth harmonics, the optimal trade-off appears to be at  $k^A = 0.2$ , where both harmonics present an EMI reduction that can be evaluated in about  $-5$  dB.

#### IV. DOUBLE TRIANGULAR MODULATION

The DTM approach recalls the method presented in [29], and it consists of superimposing slow and fast driving signals to address the trade-off between EMI reduction for the lower and for the upper part of the spectrum. In practice, this lead to consider the cascade of two FMs.

Let us define the normalized periodic driving signals  $-1 \leq g^A(\xi) \leq 1$  and  $-1 \leq g^B(\xi) \leq 1$ , both periodic with unitary angular frequency, and apply a first spreading according to frequency deviation  $k^A \Delta f$  and the driving signal  $g^A(2\pi f_m^A t + \varphi^A)$ , and a second one with frequency deviation  $k^B \Delta f$  and the driving signal  $g^B(2\pi f_m^B t + \varphi^B)$ . The first modulation leads to a change of the instantaneous phase from  $\phi(t) = 2\pi f_c t$  to

$$\phi'(t) = \phi(t) + 2\pi k^A \Delta f \int_{-\infty}^t g^A(2\pi f_m^A \tau + \varphi^A) d\tau, \quad (12)$$

whereas when adding also the spreading due to the  $g^B$  we get

$$\begin{aligned} \phi''(t) &= \phi'(t) + 2\pi k^B \Delta f \int_{-\infty}^t g^B(2\pi f_m^B \tau + \varphi^B) d\tau = \\ &= \phi(t) + 2\pi \Delta f \int_{-\infty}^t (k^A g^A(2\pi f_m^A \tau + \varphi^A) + \\ &\quad + k^B g^B(2\pi f_m^B \tau + \varphi^B)) d\tau. \end{aligned} \quad (13)$$

In other words, considering two cascading FMs is equivalent to consider a standard FM using the weighted sum of the two driving signals as new driving signal. By setting  $k^A + k^B = 1$  we may have a fair comparison between the standard triangular spreading approach with this one, as in both cases the instantaneous frequency ranges from  $f_c - \Delta f$  to  $f_c + \Delta f$ .

**Fourier spectrum.** Let us define the two auxiliary functions  $G^A$  and  $G^B$ , as well as the two sequence  $\Gamma_l^A$  and  $\Gamma_l^B$

$$\begin{aligned} G^{\{A,B\}}(\tau) &= \int_{-\infty}^{\tau} g^{\{A,B\}}(\xi) d\xi, \\ \Gamma_l^{\{A,B\}}(m) &= \int_{-\pi}^{\pi} e^{jmG^{\{A,B\}}(\tau)} e^{-jl\tau} d\tau. \end{aligned} \quad (14)$$

Proceeding as in (8), it is possible to write the modulation of a sinusoidal tone as

$$\begin{aligned} &\cos \left( 2\pi f_c t + 2\pi \Delta f \int_{-\infty}^t (k^A g^A(2\pi f_m^A \tau + \varphi^A) + \right. \\ &\quad \left. + k^B g^B(2\pi f_m^B \tau + \varphi^B)) d\tau \right) = \\ &= \text{Re} \left( e^{j2\pi f_c t} e^{jk^A m^A G^A(2\pi f_m^A t + \varphi^A)} \cdot \right. \\ &\quad \left. \cdot e^{jk^B m^B G^B(2\pi f_m^B t + \varphi^B)} \right) = \\ &= \text{Re} \left( e^{j2\pi f_c t} \sum_{l=-\infty}^{+\infty} \Gamma_l^A(k^A m^A) e^{jl\varphi^A} e^{j2\pi l f_m^A t} \cdot \right. \\ &\quad \left. \cdot \sum_{l=-\infty}^{+\infty} \Gamma_l^B(k^B m^B) e^{jl\varphi^B} e^{j2\pi l f_m^B t} \right). \end{aligned} \quad (15)$$

where we have implicitly defined  $m^{\{A,B\}} = \Delta f / f_m^{\{A,B\}}$ .

The two sums in the last line of (15) can be simplified by means of a discrete convolution involving the two sequences  $\Gamma_l^A$  and  $\Gamma_l^B$ . Let us consider, for the sake of simplicity, that  $f_m^B$  is a multiple of  $f_m^A$ , so that we define  $f_m = f_m^A = f_m^B / N$ ,  $N \in \mathbb{N}$ . Let  ${}^{(N)}\Gamma_p^B$  be the up-sampled version of  $\Gamma_l^B$ , defined as:

$${}^{(N)}\Gamma_p^B(\xi) = \begin{cases} \Gamma_l^B(\xi) & \text{if } p = Nl \\ 0 & \text{otherwise} \end{cases}. \quad (16)$$

With this, the product of the two sums can be written as:

$$\begin{aligned} &\sum_{l=-\infty}^{+\infty} \Gamma_l^A(k^A m^A) e^{jl\varphi^A} e^{j2\pi l f_m t} \cdot \\ &\quad \cdot \sum_{p=-\infty}^{+\infty} {}^{(N)}\Gamma_p^B(k^B m^B) e^{j\frac{p}{N}\varphi^B} e^{j2\pi p f_m t} = \\ &= \sum_{q=-\infty}^{+\infty} \sum_{p=-\infty}^{+\infty} \Gamma_{q-p}^A(k^A m^A) e^{j(q-p)\varphi^A} \cdot \\ &\quad \cdot {}^{(N)}\Gamma_p^B(k^B m^B) e^{j\frac{p}{N}\varphi^B} e^{j2\pi q f_m t} = \\ &= \sum_{q=-\infty}^{+\infty} \Gamma_q^* e^{j2\pi q f_m t}, \end{aligned} \quad (17)$$

where we have set  $l = q - p$ , and the sequence  $\Gamma_q^*$  has been implicitly defined as the discrete convolution between the two sequences  $\Gamma_l^A(k^A m^A) e^{jl\varphi^A}$  and  ${}^{(N)}\Gamma_p^B(k^B m^B) e^{j\frac{p}{N}\varphi^B}$  (i.e., the up-sampled version of  $\Gamma_l^B(k^B m^B) e^{jl\varphi^B}$ ). Equation (15) can now be rewritten as

$$\begin{aligned} &\text{Re} \left( e^{j2\pi f_c t} \sum_{q=-\infty}^{+\infty} \Gamma_q^* e^{j2\pi q f_m t} \right) = \\ &= \sum_{q=-\infty}^{+\infty} |\Gamma_q^*| \cos(2\pi f_c t + 2\pi q f_m t + \arg(\Gamma_q^*)). \end{aligned} \quad (18)$$

This result provides a valuable alternative to the direct computation of the  $\Gamma_l(m)$  coefficients for the FM using as driving signal the waveform  $g(\xi) = k^A g^A(\xi) + k^B g^B(\xi)$ , shown in Figure 3. In fact, owing to the assumption  $f_m = f_m^A = f_m^B / N$ , the  $g(\xi)$  is periodic with period  $1/f_m^A$ , and one may in principle consider the straightforward computation of the  $\Gamma_l(m)$  coefficients via (7). However, deriving an analytical expression requires solving a non-trivial integral in closed form, which is not always possible, or anyway proven to be a cumbersome task even if for simple cases such as the sinusoidal or triangular well-known cases.

The proposed DTM approach assumes that both  $g^A$  and  $g^B$  are triangular functions, defined as in (9). Therefore,  $\Gamma_l^A$  and  $\Gamma_l^B$  can be expressed as in [28], and  $\Gamma_q^*$  can be computed. An example comparing the expected spectrum from (18) and the spectrum simulated on Matlab is depicted in Figure 6 with  $f_m^A = 1$  kHz,  $f_m^B = 10$  kHz,  $\Delta f = 15$  kHz and  $k^A = k^B = 0.5$ . The phases of the triangular waveforms are set to  $\varphi^A = \varphi^B = \pi/2$  so that  $g^A$  and  $g^B$  have the same definition of the triangular waveforms of Figures 1 and 3, and their sum (i.e., the overall modulating waveform) is symmetric, generating a symmetric spectrum. Figure 6 shows the amplitude spectrum when the driving signal is given

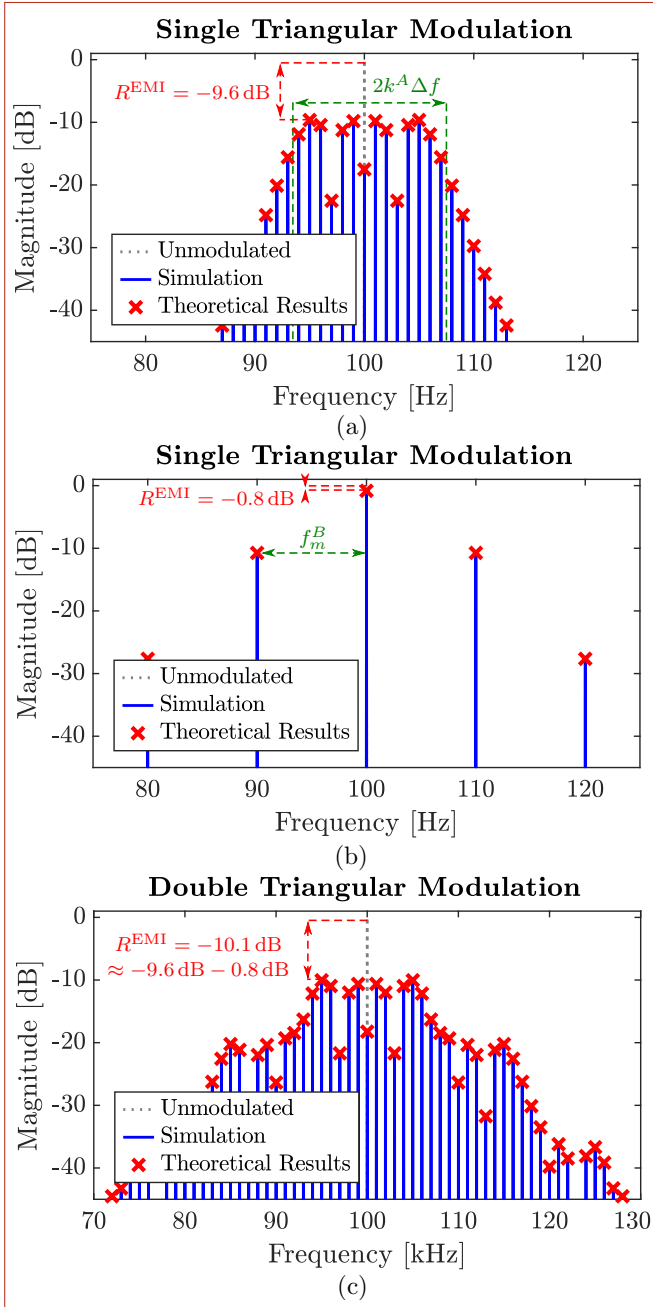


Fig. 6. Comparison between Fourier spectra computed according to (8) and (18), and that achieved by means of a Matlab simulation when the driving signal and frequency deviation are: (a)  $g^A(2\pi f_m^A t + \varphi^A)$ , and  $k^A \Delta f$ ; (b)  $g^B(2\pi f_m^B t + \varphi^B)$ , and  $k^B \Delta f$ ; (c) the weighted sum of the two functions as in (13) and  $\Delta f$ . Parameters are:  $f_c = 100$  kHz,  $f_m^A = 1$  kHz,  $f_m^B = 10$  kHz,  $\Delta f = 15$  kHz,  $k^A = k^B = 0.5$ , and  $\varphi^A = \varphi^B = \pi/2$ . The 0 dB reference level corresponds to the peak amplitude value of the unmodulated sinusoidal tone.

by  $g^A(2\pi f_m^A t + \varphi^A)$  with a frequency deviation  $k^A \Delta f$ , by  $g^B(2\pi f_m^B t + \varphi^B)$  with frequency deviation  $k^B \Delta f$ , and by the weighted sum of these two functions and with a frequency deviation  $\Delta f$ . Note that the derivation of the final spectrum as the convolution of the two individual spectra generated by  $g^A$  and  $g^B$  can be inferred also by only looking at the amplitude spectrum in the figure.

Note that, being (18) computed as the frequency modulation of a unitary amplitude sinusoidal tone, it is intuitive that the value of  $\max_q |\Gamma_q^*|$  is nothing more than the EMI reduction achieved with this modulation. If one is interested only in the EMI reduction value, the full computation of the spectrum may be not necessary. In particular, in many practical cases (e.g., if  $f_m^B$  is of the same order of  $k^A \Delta f$ , as in the case of Figure 6) the value in the convolution giving rise to the  $\Gamma_q^*$  is dominated by a single term and can be approximated as  $\max_q |\Gamma_q^*| \approx \max_l |\Gamma_l^A| \cdot \max_l |\Gamma_l^B|$  independently of  $\varphi^A$  and  $\varphi^B$ . In other words, in these cases, it is enough to consider the combination of the two peak reductions of the two individual modulations to get the peak reduction in the combined modulation. If the above hypothesis is not satisfied and multiple terms are not negligible in the computation of the convolution, the value obtained represents only an approximation (more precisely, an overestimation) of the peak reduction.

**EMI spectrum:** the complexity of the computation of the EMI measured spectrum achieved when using the sum of two driving signals appears to be overwhelming, and it is not possible to provide here an analytical solution as in the case of the Fourier spectrum. Indeed, it is reasonable assuming that all the observations we made for the Fourier spectrum apply also in this case, or at least may be used to approximate the system behavior.

Experimentally, the EMI spectrum of the combination of the two modulations can be roughly estimated by the convolution of the two individual EMI spectra. Note that this cannot be more than a rough estimation since in the EMI spectrum all information regarding the phase of any spectral component is missing. Furthermore, single tones will always appear in the measured EMI spectrum with a width equal to the RBW, but the mathematical convolution of two of them erroneously results in a spectrum with a width equal to the  $2 \cdot$  RBW.

In Figure 7, given the same parameters considered in Figure 6, we have plotted the measured EMI spectrum for the triangular modulation using  $g^A(2\pi f_m^A t + \varphi^A)$  as driving signal and  $k^A \Delta f$  as frequency deviation, the triangular modulation using  $g^B(2\pi f_m^B t + \varphi^B)$  and  $k^B \Delta f$ , and the DTM given by the weighted sum of the two functions and  $\Delta f$ . We have exploited the same measurement setup described in Section III setting, in this specific case, a fixed 1 kHz RBW.

The measured spectra, when  $g^A$  and  $g^B$  are used individually, have been compared with the expected values calculated according to [28]. In the third plot, the driving signal is the weighted sum of  $g^A$  and  $g^B$ , and the measured spectrum is compared with the convolution of the two aforementioned expected EMI spectra. In this case, we have used a normalization factor (necessary due to the fact that we are dealing with two continuous spectra) such that the convolution of two 0 dBm tones is still a 0 dBm tone. The good matching

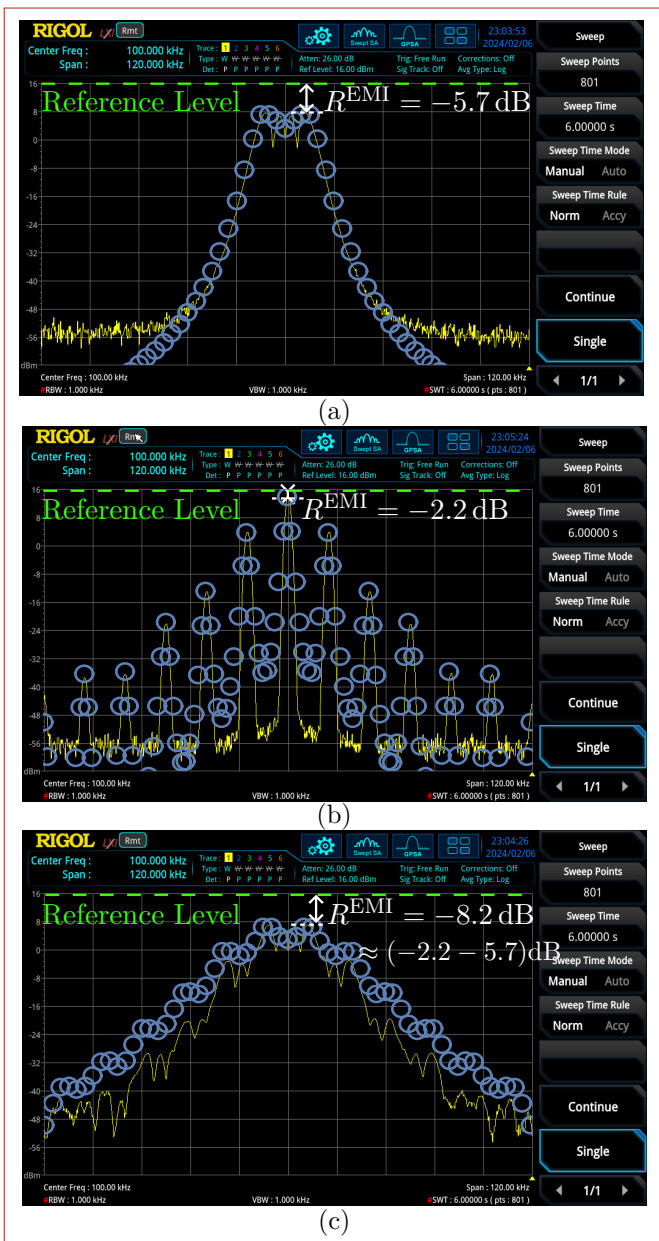


Fig. 7. Comparison between measured EMI spectra (yellow line) and that achieved using the model developed in [28] (blue-circle markers) when the driving signal and frequency deviation respectively are: (a):  $g^A(2\pi f_m^A t + \varphi^A)$ , and  $k^A \Delta f$ ; (b):  $g^B(2\pi f_m^B t + \varphi^B)$ , and  $k^B \Delta f$ ; (c): the weighted sum of the two functions as in (13) and  $\Delta f$ . Parameters are the same of Figure 6. The 16 dBm reference level (green dashed line) corresponds to the peak amplitude value of the unmodulated sinusoidal tone, while the white dashed line locates the peak amplitude of the displayed spectrum.

suggests that the aforementioned assumptions are reasonable. Given this, similarly to the case when the Fourier spectrum is considered (and, of course, under the same hypotheses), we may estimate the EMI reduction in the combined modulation as the combination of the two EMI reductions of the two individual modulations.

**Multi-RBW's Optimization:** Similarly to the STM case, sweeping the two parameters  $k^A$  and  $k^B = 1 - k^A$  allows to investigate the multi-RBW's optimization trade-off. Indeed, differently from the STM case discussed in Section III, the

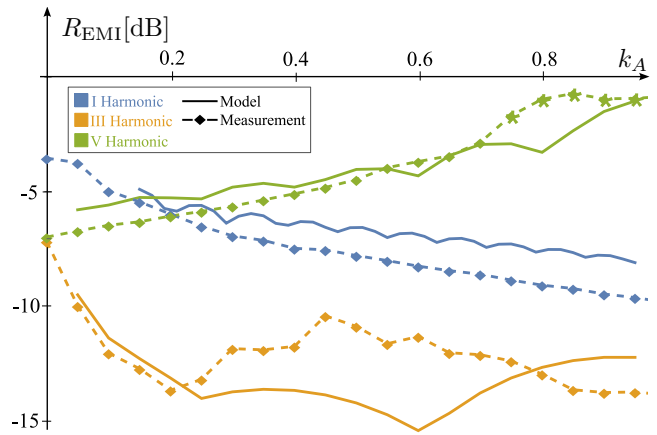


Fig. 8. Comparison between expected and measured performance for the EMI reduction of the first, third and fifth harmonic considering a DTM. Solid lines represent the reduction according to Equation (19), whereas dotted lines according to measurements.

two parameters now entails the subdivision of the overall  $\Delta f$  between  $g^A$  and  $g^B$ .

Therefore, based on the main results derived here, the EMI reduction observed for a modulated  $n$ -th harmonic can be approximated with

$$R^{EMI}(k^A m^A, \rho/k^A) \cdot R^{EMI}(k^B m^B, \rho/k^B) = R^{EMI}\left(\frac{k^A n \Delta f}{f_m^A}, \frac{RBW^{A|B}}{k^A n \Delta f}\right) \cdot R^{EMI}\left(\frac{(1-k^A)n \Delta f}{f_m^B}, \frac{RBW^{A|B}}{(1-k^A)n \Delta f}\right), \quad (19)$$

where  $RBW^{A|B}$  is set to either  $RBW^A$  or  $RBW^B$ , depending on whether the EMI reduction is being analyzed in the lower or upper part of the spectrum.

**Experimental Validation:** The EMI reduction achievable with the DTM method in (19) has been plotted with solid lines in Figure 8, considering the same set of parameters as in the STM case. In the same figure, the measured EMI reduction has also been plotted. Some discrepancies between the expected and the measured reduction are present, in particular for the third harmonic. Anyway, in general terms, the difference is limited and the reduction computed as in (19) can be effectively used as a good approximation for the DTM case.

Also in this case the trade-off is clear, and the value  $k^A = 0.2$  ensures an almost  $-5$  dB reduction both on the first and on the fifth harmonics. These parameters are very similar to the ones resulting from the STM trade-off.

## V. PERFORMANCE COMPARISON AND FINAL REMARKS

In Section III and IV, the performance results of the STM and DTM EMI reduction approaches have been respectively evaluated. Actually, the considered parameters are not relevant for real EMI measurements, as we should have considered  $RBW^A = 9$  kHz and  $RBW^B = 120$  kHz, and a value of  $f_c$  in the order of a few MHz. Due to some limitation in the measurement setup, we have preferred to consider a re-scaled parameter system, where however the ratio between the two considered RBWs is similar to that one can find in an EMI relevant setting, suggesting that the conclusions we draw in our setting will be applicable also to the relevant setting.

The more obvious observation when comparing results of Figure 5 and 8 is that performance are not so different, in particular for the first and fifth harmonics. Limiting to the third harmonic, the DTM approach appears to achieve slightly better results. Indeed, even if generalization from a simple case study is dangerous in many situations, there are no clues here to argue that this is not the general trend. In both figures it is obvious that the points  $k^A = 0$  and  $k^A = 1$  for both cases are the same, corresponding to two simple triangular spreading at  $f_m^A$  and  $f_m^B$ , respectively. Around these points, all the curves of the two approaches are overlapping. Since the trend, when increasing  $k^A$  from 0 to 1, is not so far from a linear trend, no large differences between the two approaches are expected for other parameters value, including that of a EMI relevant setting.

If the two approaches are similar in terms of performance, the comparison should be moved in terms of hardware complexity. It is intuitive that the complexity of generating two triangular driving signals is indeed higher than the complexity of generating a single triangular driving signal. However, a fair comparison requires many additional hardware considerations, that are generally different from case to case. As a simple example, the assumption of a digitally implemented modulation mitigate the overwhelming complexity of the DTM approaches. If instead we assume an analog implementation, one of the most problematic aspect is the bandwidth of the modulation system that has to be large enough not to generate distortion in the driving signal. In this case the DTM is more problematic, as we need to deal with a triangular signal with frequency  $f_m^B$ , whereas in the simpler case we have a lower frequency given by  $k^A f_m^A + k^B f_m^B$ . It may be worth nothing that in the scenario considered in the paper, optimization requires  $k^A = 0.2$ , so that the difference in required bandwidth for the two cases is negligible. Anyway, since the hardware complexity comparison is strongly dependent on the available hardware, we consider it out of the scope of this paper.

## VI. CONCLUSION

In this paper we have considered two different trade-offs in the optimization of the EMI reduction when using the spread spectrum clocking in an environment where some interfering signal harmonics require to be analyzed with a lower RBW, and some others with a higher RBW. Limiting ourselves to triangular driving signals allows us to provide a theoretical framework to evaluate the expected EMI reduction in this environment, and to compare it with measured performance. A simple approach where a single triangular driving signal is used, if properly optimized, is capable to achieve an EMI reduction similar to that achieved by a much more complex approach, where two triangular driving signals (one at lower frequency, one at higher frequency) are used, making questionable the adoption of the more complex modulation scheme.

## REFERENCES

[1] F. Lin and D. Chen, "Reduction of power supply EMI emission by switching frequency modulation," *IEEE Trans. Power Electron.*, vol. 9, no. 1, pp. 132–137, Jan. 1994. doi: 10.1109/63.285504

[2] K. Hardin, J. Fessler, and D. Bush, "Spread spectrum clock generation for the reduction of radiated emissions," in *Proceedings of IEEE symposium on electromagnetic compatibility*, Aug. 1994, pp. 227–231. doi: 10.1109/ISEMC.1994.385656

[3] "Code of Federal Regulations. Title 47 (47CFR), part 15, subpart B: "Unintentional Radiators"."

[4] "Council Directive on the approximation of the laws of the Member States relating to electromagnetic compatibility (89/336/EEC)," May 1989.

[5] "Electromagnetic compatibility of multimedia equipment - Emission requirements (CISPR 32:2015)," 2015.

[6] D. De Caro, G. Di Meo, E. Napoli, N. Petra, and A. G. M. Strollo, "A 1.45 GHz all-digital spread spectrum clock generator in 65nm CMOS for synchronization-free SoC applications," *IEEE Transactions on Circuits and Systems I: Regular Papers*, vol. 67, no. 11, pp. 3839–3852, Nov. 2020. doi: 10.1109/TCSI.2020.3008481

[7] M. Leoncini *et al.*, "Spread-spectrum frequency modulation in a DC/DC converter with time-based control," *IEEE Transactions on Power Electronics*, vol. 38, no. 4, pp. 4207–4211, Apr. 2023. doi: 10.1109/TPEL.2022.3227954

[8] T.-W. Sun, M.-Z. Li, T.-H. Tsai, and C.-C. Chang, "A high-accuracy hysteretic DC-DC converter using a spread-spectrum EMI suppression technique with double gold codes," in *2023 21st IEEE inter-regional NEWCAS conference (NEWCAS)*, Jun. 2023, pp. 1–4. doi: 10.1109/NEWCAS57931.2023.10198156

[9] E. Stok, M. Otten, H. Huisman, and Y. Kösesoy, "EMI reduction in an interleaved buck converter through spread spectrum frequency modulation," in *2023 25th european conference on power electronics and applications (EPE'23 ECCE europe)*, Sep. 2023, pp. 1–11. doi: 10.23919/EPE23ECCEurope58414.2023.10264338

[10] F. Pareschi, R. Rovatti, and G. Setti, "EMI Reduction via Spread Spectrum in DC/DC Converters: State of the Art, Optimization, and Tradeoffs," *IEEE Access*, vol. 3, pp. 2857–2874, 2015. doi: 10.1109/ACCESS.2015.2512383

[11] P. Mathur and S. Raman, "Electromagnetic interference (EMI): Measurement and reduction techniques," *Journal of Electronic Materials*, vol. 49, no. 5, pp. 2975 – 2998, 2020. doi: 10.1007/s11664-020-07979-1

[12] M. Yanuar H, R. Hidayat, and E. Firmansyah, "An experimental study of conducted EMI mitigation on the LED driver using spread spectrum technique," *International Journal of Electronics and Telecommunications*, vol. vol. 62, no. No 3, 2016. doi: 10.1515/leletel-2016-0041

[13] M. Y. Hariyawan, R. Hidayat, and E. Firmansyah, "The Effects of spread spectrum techniques in mitigating conducted EMI to LED luminance," *International Journal of Electrical and Computer Engineering*, vol. 6, no. 3, pp. 1332 – 1343, 2016. doi: 10.11591/ijee.v6i3.9528

[14] M. Kim, H.-P. Park, and J.-H. Jung, "Spread spectrum technique with random-linear modulation for EMI mitigation and audible noise elimination in IH appliances," *IEEE Transactions on Industrial Electronics*, vol. 69, no. 8, pp. 8589–8593, Aug. 2022. doi: 10.1109/TIE.2021.3102405

[15] H. Alsuraistry *et al.*, "A 6-GHz spread spectrum clock generation with EMI reduction of 30.2 dB for SATA-III applications," *Microwave and Optical Technology Letters*, vol. 59, no. 3, pp. 622–624, 2017. doi: 10.1002/mop.30359

[16] D. Yan and D. B. Ma, "An automotive-use battery-to-load GaN-Based switching power converter with anti-aliasing MR-SSM and in-cycle adaptive ZVS techniques," *IEEE Journal of Solid-State Circuits*, vol. 56, no. 4, pp. 1186–1196, Apr. 2021. doi: 10.1109/JSSC.2020.3040147

[17] Y. Chen and D. B. Ma, "EMI-Regulated GaN-Based switching power converter with markov continuous random spread-spectrum modulation and one-cycle on-Time rebalancing," *IEEE Journal of Solid-State Circuits*, vol. 54, no. 12, pp. 3306–3315, Dec. 2019. doi: 10.1109/JSSC.2019.2931439

[18] Y. Shan *et al.*, "Space spread-spectrum strategy for MMC to reduce the conducted EMI," *IEEE Transactions on Industrial Electronics*, vol. 69, no. 11, pp. 10807–10818, Nov. 2022. doi: 10.1109/TIE.2021.3125656

[19] J. Kundra, I. Skeledzija, and A. Baric, "EMI and voltage ripple co-optimization of a spread-spectrum controller in buck converters," *IEEE Access*, vol. 10, pp. 131909–131919, 2022. doi: 10.1109/ACCESS.2022.3229972

[20] C.-H. Moon, C.-J. Chen, and S.-W. Lee, "A random modulation spread-spectrum digital PWM for a low system clock digital buck converter," *IEEE Access*, vol. 9, pp. 156663–156671, 2021. doi: 10.1109/ACCESS.2021.3126556

[21] *ALDD7709 - Automotive LED driver 4-channel 200 mA with a DC-DC controller*. STMicroelectronics Datasheet DS14214 - Rev 4, Jun. 2023.

- [22] *L6983 - 38 V, 3 A synchronous step-down converter with 17  $\mu$ A quiescent current*. STMicroelectronics Datasheet DS13116 - Rev.3, Dec. 2022.
- [23] H. S. Black, *Modulation theory*. Van Nostrand, 1953.
- [24] F. Pareschi, G. Setti, R. Rovatti, and G. Frattini, "Short-term Optimized Spread Spectrum Clock Generator for EMI Reduction in Switching DC/DC Converters," *IEEE Trans. Circuits Syst. I, Reg. Papers*, vol. 61, no. 10, pp. 3044–3053, Oct. 2014. doi: 10.1109/TCSI.2014.2327273
- [25] G. Setti, M. Balestra, and R. Rovatti, "Experimental verification of enhanced electromagnetic compatibility in chaotic fm clock signals," in *2000 IEEE International Symposium on Circuits and Systems (ISCAS)*, vol. 3, 2000, pp. 229–232 vol.3. doi: 10.1109/ISCAS.2000.856038
- [26] D.-S. Shen and S.-I. Liu, "A low-jitter spread spectrum clock generator using FDMP," *IEEE Transactions on Circuits and Systems II: Express Briefs*, vol. 54, no. 11, pp. 979–983, 2007. doi: 10.1109/TC-SII.2008.919993
- [27] H.-H. Chang, I.-H. Hua, and S.-I. Liu, "A spread-spectrum clock generator with triangular modulation," *IEEE Journal of Solid-State Circuits*, vol. 38, no. 4, pp. 673–676, 2003. doi: 10.1109/JSSC.2003.809521
- [28] F. Pareschi, G. Setti, R. Rovatti, and G. Frattini, "Practical Optimization of EMI Reduction in Spread Spectrum Clock Generators With Application to Switching DC/DC Converters," *IEEE Trans. Power Electron.*, vol. 29, no. 9, pp. 4646–4657, Sep. 2014. doi: 10.1109/TPEL.2013.2286258
- [29] P. Curtis and E. Lee, *EMI Reduction Technique, Dual Random Spread Spectrum*. Texas Instruments Application Note SNVA974A, Jun. 2020.
- [30] S. Callegari, R. Rovatti, and G. Setti, "Spectral properties of chaos-based FM signals: theory and simulation results," *IEEE Transactions on Circuits and Systems I: Fundamental Theory and Applications*, vol. 50, no. 1, pp. 3–15, Jan. 2003. doi: 10.1109/TCSI.2002.807510